Coverage-based treatment planning to accommodate deformable organ variations in prostate cancer treatment

Huijun Xu[a)]
Department of Radiation Oncology, Virginia Commonwealth University, Richmond, Virginia 23298 and Department of Radiation Oncology, University of Maryland, Baltimore, Maryland 21201

Douglas J. Vile and Manju Sharma
Department of Radiation Oncology, Virginia Commonwealth University, Richmond, Virginia 23298

J. James Gordon
Department of Radiation Oncology, Henry Ford Health System, Detroit, Michigan 48202

Jeffrey V. Siebers
Department of Radiation Oncology, Virginia Commonwealth University, Richmond, Virginia 23298 and Department of Radiation Oncology, University of Virginia, Charlottesville, Virginia 22908

(Received 5 September 2013; revised 11 July 2014; accepted for publication 14 July 2014; published 24 September 2014)

Purpose: To compare two coverage-based planning (CP) techniques with standard fixed margin-based planning (FM), considering the dosimetric impact of interfraction deformable organ motion exclusively for high-risk prostate treatments.
Methods: Nineteen prostate cancer patients with 8–13 prostate CT images of each patient were used to model patient-specific interfraction deformable organ changes. The model was based on the principal component analysis (PCA) method and was used to predict the patient geometries for virtual treatment course simulation. For each patient, an IMRT plan using zero margin on target structures, prostate ($CTV_{prostate}$) and seminal vesicles (CTV_{SV}), were created, then evaluated by simulating 1000 30-fraction virtual treatment courses. Each fraction was prostate centroid aligned. Patients whose D_{98} failed to achieve 95% coverage probability objective $D_{98,95} \geq 78$ Gy ($CTV_{prostate}$) or $D_{98,95} \geq 66$ Gy (CTV_{SV}) were replanned using planning techniques: (1) FM ($PTV_{prostate} = CTV_{prostate} + 5$ mm, $PTV_{SV} = CTV_{SV} + 8$ mm), (2) CP_{OM} which optimized uniform PTV margins for $CTV_{prostate}$ and CTV_{SV} to meet the coverage probability objective, and (3) CP_{COP} which directly optimized coverage probability objectives for all structures of interest. These plans were intercompared by computing probabilistic metrics, including 5% and 95% percentile DVHs (pDVH) and TCP/NTCP distributions.
Results: All patients were replanned using FM and two CP techniques. The selected margins used in FM failed to ensure target coverage for 8/19 patients. Twelve CP_{OM} plans and seven CP_{COP} plans were favored over the other plans by achieving desirable $D_{98,95}$ while sparing more normal tissues.
Conclusions: Coverage-based treatment planning techniques can produce better plans than FM, while relative advantages of CP_{OM} and CP_{COP} are patient-specific. © *2014 American Association of Physicists in Medicine.* [http://dx.doi.org/10.1118/1.4894701]

Key words: coverage, treatment planning, IMRT optimization, deformable motions, PCA, prostate cancer

1. INTRODUCTION

Geometric uncertainties (GUs) should be adequately considered during the treatment planning process of external beam radiation therapy. GUs, in the form of delineation uncertainties, setup errors, interfraction and intrafraction organ variations may prevent one from achieving the therapeutic intent of treatment by introducing deviations between the planned (intended) and the treatment geometry. For prostate cancer treatment, interfraction organ displacement and deformation are primarily due to differential bladder and rectal filling, which can vary significantly during the treatment course.[1–5]

To account for GUs, conventional planning applies safety margins to the clinical target volumes (CTVs) to create surrogate planning target volumes (PTVs) for treatment planning.[6,7] An ideal PTV margin ensures CTV coverage while maximally sparing the surrounding dose-limiting organs at risk (OARs) (i.e., bladder and rectum). However, the PTV margin is not easily determined for organ deformation and motion. One reason is that the characteristics of organ deformable motions are complex. In contrast to rigid organ motion and setup errors that can be described by six parameters comprising of shifts and rotations, organ deformable motions are of a much higher dimensionality. Therefore, the commonly used margin recipes[8,9] derived for rigid motion are at best approximate when used to accommodate deformations. Another reason is that the dosimetric consequence of a margin may vary with factors such as patient and plan

quality and conformity. Although PTV margins to account for prostate and seminal vesicle interfractional variations have been suggested,[10,11] they are population based and therefore should be used with caution for each patient.

As advanced techniques for target localization and plan adaptation to reduce GUs have not become clinical routine procedure (due in part to its complexity, and in part to the clinical time demands), an intermediate solution can be found in coverage-based treatment planning (CP) techniques. Such techniques utilize GU models to evaluate a quantity called coverage probability, which is the probability that a realized target or OAR dose metric D_v exceeds the dose of interest (Rx, tolerance or other dose) when treatment planning and delivery uncertainties are taken into account.[12] By evaluating and optimizing coverage probability-based objectives, CP optimization techniques optimize the beam-fluences to ensure that a prespecified percentage (e.g., 95%) of probable patient treatment courses will meet the plan dosimetric criteria.

Our research group has developed two CP techniques—optimized-margin planning (CP_{OM})[13] and coverage-optimized planning (CP_{COP}).[14] CP_{OM} is an iterative approach which modifies PTV margins until predefined coverage criteria are satisfied, while CP_{COP} does away with the PTV and modifies dosimetric "margins" between CTV and treated volume (the volume enclosed by a critical isodose surface[7]) until the coverage criteria are satisfied. In the presence of (rigid-body) setup errors, both CP_{OM} and CP_{COP} showed advantages relative to conventional PTV-based planning for prostate cancer patients. Using CP_{OM} for translation setup errors following a Gaussian distribution with standard deviation (SD) of 2 mm for systematic and random errors, the total volume of normal tissue receiving dose higher than 65 Gy was reduced on average by 19.3% or about 48 cm^3.[13] For translation setup errors following a Gaussian distribution with systematic and random SD 3 mm, using CP_{COP} was more likely to achieve CTV prescribed dose when OAR dose was below the optimization limits.[14] However, the clinical advantages due to using CP_{OM} or CP_{COP} to accommodate the deformable organ motions have not been studied.

To explore potential advantages of CP based optimization, a representative GU model for simulating deformable organ motion is required. Many mathematical models have been developed.[11,15–20] Among these models, principal component analysis (PCA) was found to be an efficient and powerful model.[19,21] PCA compresses large and unorganized deformation data (e.g., from observations) to a low-dimensional system of basis vectors. These vectors, also called eigenmodes, are ranked according to their contribution to the deformation. The residual errors of a patient-specific PCA model for prostate, bladder, and rectum were small, e.g., less than 2 mm when eigenmodes representing more than 86% overall variability were used.[19] (For population based variability, additional dominate eigenmodes are required.[20]) PCA models have been implemented to estimate geometric coverage probabilities[22] and to evaluate the dosimetric consequence of virtual treatment courses[21] for prostate patients. However, to date, the implementation of PCA models has not been utilized for coverage-based plan optimization.

In this work, the prostate treatment plans were created to exclusively account for the interfraction organ deformation and translation simulated by a patient-specific PCA model. The plans using fixed margin-based planning (FM), CP_{COP}, and COP_{OM} are intercompared to investigate the potential clinical benefit of CP techniques.

2. METHODS

2.A. Prostate plans

Prostate image sets provided by the Netherlands Cancer Institute were used in this study. The patients' characteristics were described by Deurloo *et al.*,[23] while the images and image processing were described by Sharma *et al.*[24] In summary, the image sets provided were bony-anatomy aligned and included an initial planning fan-beam computed tomography (CT) and multiple repeat fan-beam CTs (rCT, N_{rCT} = 7–12) acquired throughout the 7–8 week course of radiotherapy. For each CT image, the structures including prostate, seminal vesicles, rectum, bladder, left femur, and right femur were delineated by a single physician at VCU. All patients were assumed to have high-risk prostate cancer for the purposes of this study. The target volumes, CTVs, were the prostate ($CTV_{prostate}$) and the seminal vesicles (CTV_{SV}). No associated lymph nodes were included. The remaining contoured structures (bladder, rectum, etc.) were regarded as OARs, while the left and right femurs and the small bowel were excluded since their dose limits are rarely violated due to being more distant from the CTVs than the bladder and rectum.

For each patient, the first CT image was selected as the reference image set for planning. All of the IMRT plans utilized seven coplanar beams in the patient's transverse plane, with gantry angles 30°, 80°, 130°, 180° (posterior), 230°, 280°, and 330° with the isocenter at the prostate centroid.

Table I lists the in-house IMRT criteria protocols used for the technique that was dependent (FM or CP_{OM}) or independent (CP_{COP}) of the PTV margins, respectively. The prescription dose 78 Gy to $CTV_{prostate}$ was planned assuming 30 treatment fractions. For CP_{COP} plans, 95% and 5% coverage value were selected for minimum or maximum probabilistic DVH (pDVH) criteria to achieve static dose–volume criteria (used for FM or CP_{OM}) for 95% of the treatment courses simulated. The norm_tissue_ring was an artificial structure extending from 7 to 30 mm from $CTV_{prostate}$ and CTV_{SV} to force a steep dose drop-off. Exclusively for the implementation of CP_{COP} for some treatment planning system (TPS), CTV_neighborhood was required to set the initial beam fluence. Here, CTV_neighborhood was defined as a virtual target expansion extending 12 mm from the union volume of $CTV_{prostate}$ and CTV_{SV} on all image sets. This structure did not play an active role during optimization due to the zero objective weight.

All optimizations were performed using the Pinnacle[3] (Version 9.100) TPS (Philips Medical Systems, Fitchburg, WI), based on direct machine parameter optimization (DMPO). The optimizer was run for maximal 50 iterations, since the

TABLE I. Optimization criteria used for (a) CP_{COP} and (b) FM and CP_{OM} plans. Doses (D) are in gray (Gy). The first subscript is percentage volume, the second the coverage value. Criterion weights are shown in square brackets. PTV1 = $CTV_{prostate}$ + $CTV_{prostate}$ PTV margin and PTV2 = CTV_{SV} + CTV_{SV} PTV margin.

(a) Optimization criteria for CP_{COP} plans	
$CTV_{prostate}$	$D_{98,95} \geq 78$ [100], $D_{2,5} \leq 81$ [50]
CTV_{SV}	$D_{98,95} \geq 66$ [100]
Bladder	$D_{70,5} \leq 18$, $D_{50,5} \leq 36$, $D_{30,5} \leq 57$, $D_{20,5} \leq 66$, $D_{14,5} \leq 69$, $D_{9,5} \leq 75$, $D_{2,5} \leq 81$ [10]
Rectum	$D_{50,5} \leq 36$, $D_{30,5} \leq 51$, $D_{20,5} \leq 66$, $D_{5,5} \leq 69$, $D_{2,5} \leq 75$ [10]
Norm_tissue_ring	(static) $D_0 \leq 60$ [1]
CTV_neighborhood	(static) $D_{25} \geq 10$ [0]
(b) Optimization criteria for FM and CP_{OM} plans	
PTV1	$D_{98} \geq 78$ [100], $D_2 \leq 81$ [50]
PTV2	$D_{98} \geq 66$ [100]
Bladder	$D_{70} \leq 18$, $D_{50} \leq 36$, $D_{30} \leq 57$, $D_{20} \leq 66$, $D_{14} \leq 69$, $D_9 \leq 75$, $D_2 \leq 81$ [10]
Rectum	$D_{50} \leq 36$, $D_{30} \leq 51$, $D_{20} \leq 66$, $D_5 \leq 69$, $D_2 \leq 75$ [10]
norm_tissue_ring	$D_0 \leq 60$ [1]

composite objective values converge quickly, with small improvements which increase plan complexity afterward. Dose grid resolution was $2\times2\times2$ mm^3 when performing plan evaluation/comparison and $3\times3\times3$ mm^3 for optimization. (See Sec. 2.C for details.)

2.B. Deformable motion models—PCA

The interfraction organ deformable motions were modeled by PCA on a patient-specific basis. The mathematics are similar to published surfaced based PCA models.[19,21,25] The interested reader is referred to the Appendix for the PCA implementation details.

The PCA model was used to produce prostate centroid aligned synthetic DVFs ($\mathbf{DVF}_{syn\_Paligned}$) (Fig. 1). These DVFs were then used to map the reference prostate CTV, bladder, and rectum to plausible anatomically deformed ROIs for the virtual treatment fractions in the CP_{OM}/CP_{COP} optimization processes. Based on the anatomical deformation information and the algorithm described in Sec. 2.C, the ROI coverage was estimated and used to optimize dose distribution which met probabilistic criteria.

2.C. Coverage estimation and coverage-based optimization

2.C.1. Coverage estimation—pDVH

One way to evaluate the effect of GUs on dose-based plan evaluation metrics is to use Monte Carlo to sample a synthetic patient anatomy then mimic dose delivery to that anatomy. By repeating the simulation $n_{frac} = 30$ times, a single treatment course is simulated, and plan evaluation metrics for that treatment course can be tallied. By repeating the treatment course simulations many (e.g., 1000) times, distributions of the plan evaluation metrics can be obtained. A major plan evaluation tool used in this study was the pDVH, which permits evaluation of coverage probability. A pDVH corresponding to coverage q is a virtual DVH created by connecting all D_v with coverage probability q. The steps to generate a pDVH for a target or CTV can be referred to Gordon *et al.*[14] In this study, a pDVH is a result of "dynamic" DVHs which are different in each virtual treatment course due to the different DVFs sampled from PDFs of PCA model.

2.C.2. Planning technique—FM

FM is a PTV-based treatment planning technique based on the conventional margin-based planning method where predefined PTV margins are determined empirically. The fixed uniform PTV margins utilized by FM in this work were

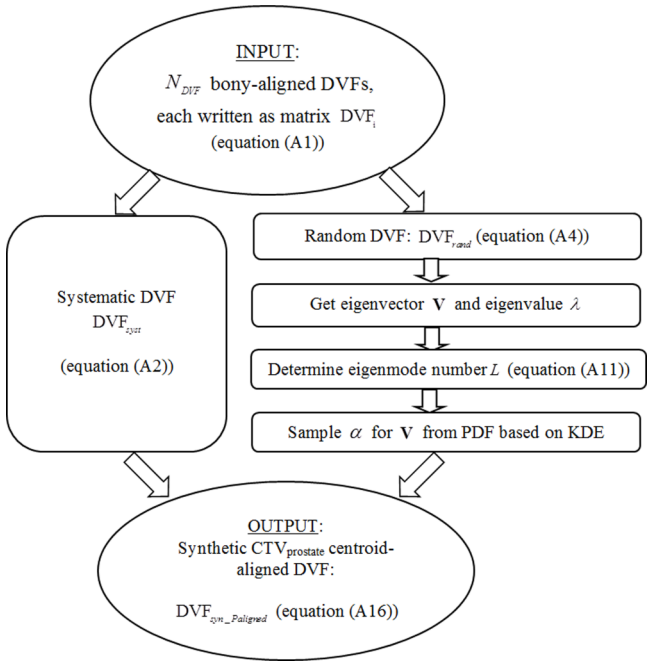

FIG. 1. The flow chart for creating a patient-specific PCA model used in the treatment simulations.

5 mm for $CTV_{prostate}$ and 8 mm for CTV_{SV} for all patients, according to a published work.[11]

2.C.3. Planning technique — CP_{COP}

CP_{COP} optimizes the dose at prescribed coverage-based on the pDVH criteria, which operate on pDVH with possible variability considered. The basic mathematics can be found in the proof-of-concept work.[14] CP_{COP} optimization is briefly described in the following paragraph.

As opposed to the conventional IMRT optimization that utilizes margin-based structures (i.e., PTV for CTV or PRV for OAR) to ensure coverage when the underlying ROI changes position and/or shape, CP_{COP} optimizes dose directly to the variable CTV/OAR. This requires adjusting fluence elements that can intersect the CTV/OAR at its varying positions (in the accelerator coordinate system), a volume call the ROI neighborhood. Similar to a PTV/PRV, the ROI neighborhood can be determined via CTV/OAR expansion or via direct knowledge of probable locations of the CTV/OAR based on simulation. The latter method was used in this work; 1000 virtual treatment courses simulations were performed and voxels covered by the "moving" CTV/OAR in any fraction of any virtual treatment course were included in the ROI neighborhood. For the planner using CP_{COP}, exact specification of the ROI neighborhood is not required. Undersizing the ROI neighborhood results in an inability to achieve CTV/OAR coverage which would be noticed and corrected for during planning. Oversizing the ROI neighborhood does not affect coverage but incrementally slows the optimization by the inclusion of noncontributing fluence elements in the optimization loop. To enhance conformity and efficiency, CP_{COP} utilizes voxel weighting factor ω_i for each ROI neighborhood voxel. As in the work of Gordon *et al.*,[14] $\omega_i = 5 \cdot P_i$ was used here with P_i being the probability of the voxel i being covered by the moving ROI.

CP_{COP} optimizes ROI dose utilizing Newton's method with pDVH-based objectives to minimize the sum of squared dose differences. For a minimum pDVH objective [criterion $\Pr[D_{C_{Rx}} \geq D_{Rx}] \geq q_{Rx}$, $D_{C_{Rx}}$ being the dose at the prescribed coverage probability q_{Rx} (e.g., 95%)] and D_{Rx} being the prescription dose), the objective function in this study was

$$f^{\text{MinpDVH}} = \frac{1}{N_{\text{ROI\_neighborhood}}} \cdot \sum_{i}^{N_{\text{ROI\_neighborhood}}} H(D_{Rx} - D_i) \cdot H(D_i - D_{C_{Rx}}) \cdot \omega_i^2 (D_i - D_{Rx})^2, \quad (1)$$

where H was Heaviside function defined as

$$H(x) = \begin{cases} 1 & (x > 0) \\ 0 & (x \leq 0) \end{cases}. \quad (2)$$

The maximum pDVH objective [criterion $\Pr[D_{C_{Rx}} \leq D_{Rx}] \geq 1 - q_{Rx}$], the objective function was

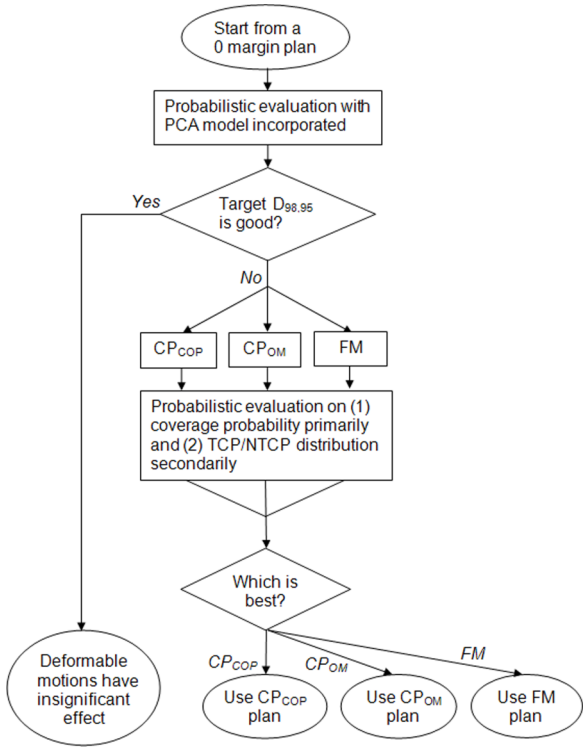

FIG. 2. Decision flow to compare the CP_{COP}, CP_{OM}, and FM techniques when plan evaluation considers the effect of deformable organ motion. The decision criteria is the target coverage, with a secondary criteria based on TCP/NTCP/P+ values.

$$f^{\text{MaxpDVH}} = \frac{1}{N_{\text{ROI\_neighborhood}}} \cdot \sum_{i}^{N_{\text{ROI\_neighborhood}}} H(D_i - D_{Rx}) \cdot H(D_{C_{Rx}} - D_i) \cdot \omega_i^2 (D_i - D_{Rx})^2. \quad (3)$$

CP_{COP} minimized the sum of a series of pDVH objectives to form the "optimized" dose using identical techniques as the dose–volume-based optimization described by Wu *et al.*[26]

Here, 100 virtual treatment courses were simulated during the optimization to save computation time and memory, which increase with the number of virtual treatment courses. (For a 50-iteration optimization, the run time for COP on a 2.93 GHz Quad Core Processor Core i7-870 is 3–4 h.) 1000 treatment courses were used for postoptimization evaluations.

2.C.4. Planning technique — CP_{OM}

Based on the work of Gordon *et al.*,[13] CP_{OM} used in this work started with 0 PTV margins for $CTV_{prostate}$ and CTV_{SV}. If the CTV(s) failed to achieve the prescribed $D_{98,95}$, PTV margin(s) was(were) iteratively increased uniformly in 1 mm increments. In the outer loop of each iteration, the $D_{98,95}$ values were estimated based on the dosimetric simulation of 1000 virtual treatment courses with the PCA model incorporated. The iteration stopped when both CTVs achieved

TABLE II. A summary of TCP and NTCP models and parameters for $CTV_{prostate}$, bladder, and rectum used in this work. Note, conventionally TCP or NTCP values are calculated for a PTV or PRV volume. Here, TCP or NTCP are computed for the base CTV or OAR volumes during the coverage simulations, yielding distributions of the parameters.

TCP: Poisson model (Refs. 27–30)	
Equation	$\mathrm{TCP} = \exp\left(-\frac{\ln 2}{N}\sum_i \exp\left[2\frac{\gamma_{50}}{\ln 2}\left(1-\frac{\mathrm{BED}_i}{D_{50}}\right)\right]\right)$ or $= \exp\left(-\ln 2 \cdot \exp\left[2\frac{\gamma_{50}}{\ln 2}\left(1-\frac{\mathrm{gBEUD}}{D_{50}}\right)\right]\right)$ where $\mathrm{BED}_i = D_i \cdot \left[1+\frac{D_i/n}{(\alpha/\beta)}\right]$ and $\mathrm{gBEUD} = \left(\sum_i \nu_i \cdot \mathrm{BED}_i^a\right)^{1/a}$
Parameters	D_{50} (dose producing 50% tumor control), γ_{50} (slope parameter), a (EUD parameter), α/β (BED parameter)
$CTV_{prostate}$ (Ref. 31)	$D_{50} = 67.5$ Gy, $\gamma_{50} = 2.2$, $a = 0.16$, $\alpha/\beta = 3$ Gy
NTCP: Lyman–Kutcher–Burman model (Refs. 32 and 33)	
Equation	$\mathrm{NTCP} = \frac{1}{\sqrt{2\pi}}\int_{-\infty}^{t} du \exp\left(-u^2/2\right)$ where $t = (\mathrm{gBEUD} - TD_{50})/(mTD_{50})$, $\mathrm{gBEUD} = \left(\sum_i \nu_i \cdot \mathrm{BED}_i^a\right)^{1/a}$ and $\mathrm{BED}_i = D_i \cdot \left[1+\frac{D_i/n}{(\alpha/\beta)}\right]$
Parameters	TD_{50} (the tolerance dose producing a 50% complication probability), m (slope parameter), a (gBEUD parameter), α/β (BED parameter)
Bladder (Refs. 34 and 35)	$TD_{50} = 80$ Gy, $m = 0.11$, $a = 20$, $\alpha/\beta = 5$ Gy
Rectum (QUANTEC)	$TD_{50} = 76.9$ Gy, $m = 0.13$, $a = 11.1$, $\alpha/\beta = 5$ Gy

their $D_{98,95}$. CP_{OM} contrasted with CP_{COP} in that CP_{OM} used standard dose–volume objectives for OAR while CP_{COP} considered OAR coverage probability during optimization and generated dosimetric margins (effectively nonuniform PTV margins) surrounding the targets in place of uniform PTV margins. Overall, CP_{OM} was less complicated and placed more emphasis on CTV coverage than CP_{COP}.

2.D. Study decision flow

A treatment planning decision flow was designed as shown in Fig. 2. This decision flow existed to address two questions (1) Whether the dosimetric effect of GUs is insignificant and (2) how to determine which plan among the three FM, CP_{OM}, and CP_{COP} plans is preferred.

2.D.1. Dosimetric effect evaluation on zero-PTV-margin plans

First, the dosimetric effect of PCA modeled deformable organ motion was evaluated on a zero-PTV-margin IMRT plan with $PTV1 = CTV_{prostate}$ and $PTV2 = CTV_{SV}$. 1000 virtual treatment courses (30 fractions per treatment course) were simulated with the PCA model to incorporate the GUs. The target dose–volume metric D_{98} at a prescribed coverage probability of 95% ($D_{98,95}$) was computed for both $CTV_{prostate}$ and CTV_{SV}. Denote $D_{98,95,Rx}$ as the prescribed dose 78 Gy for $CTV_{prostate}$ and 66 Gy for CTV_{SV}. If $D_{98,95} \geq D_{98,95,Rx}$ for both $CTV_{prostate}$ and CTV_{SV}, the dosimetric effect of deformable organ motions for this patient would have been regarded as insignificant since target coverage probability was resistant to anatomical variability. Otherwise, replanning the plan to further improve target coverage probability was required.

TABLE III. The percentage target dose degradation $\%\Delta D_{98,95}$ for $CTV_{prostate}$ (P) and CTV_{SV} (S) for zero-PTV-margin plan, and the optimized PTV margins obtained by CP_{OM} technique across 19 patients.

ID	Zero-PTV-plan $\%\Delta D_{98,95}$ (%)	CP_{OM} PTV (mm)
1	P: 4.9 S: 14.5	P: 2 S: 8
2	P: 5.8 S: 6.4	P: 10 S: 5
3	P: 5.3 S: 1.3	P: 5 S: 3
4	P: 7.7 S: 14.4	P: 5 S: 3
5	P: 1.3 S: 8.5	P: 2 S: 6
6	P: 0.8 S: 8.5	P: 1 S: 3
7	P: 2.2 S: 0.0	P: 2 S: 0
8	P: 1.7 S: 0.0	P: 4 S: 3
9	P: 2.9 S: 16.9	P: 6 S: 18
10	P: 11.1 S: 24.7	P: 7 S: 15
11	P: 9.5 S: 0.0	P: 9 S: 0
12	P: 7.5 S: 9.8	P: 9 S: 5
13	P: 2.7 S: 31.4	P: 5 S: 4
14	P: 0.8 S: 32.9	P: 4 S: 8
15	P: 0.8 S: 0.0	P: 1 S: 0
16	P: 2.4 S: 0.0	P: 2 S: 2
17	P: 3.1 S: 24.8	P: 3 S: 5
18	P: 2.6 S: 4.6	P: 4 S: 4
19	P: 0.7 S: 0.0	P: 2 S: 0

TABLE IV. Patient study ID, the preferred planning technique and the most representative gain with respect to the other two plans in terms of target dose $D_{98,95}$ for $CTV_{prostate}$ or CTV_{SV}, normal tissue coverage $D_{v,5}$ for bladder or rectum, and probability of complication free control P+. ID with */†/‡ denotes CP_{COP}/CP_{OM}/FM plan that fails to achieve target $D_{98,95}$.

ID	Best plan	Gain relative to the other plans	
1*	CP_{OM}	CP_{COP} (+0.8% $CTV_{prostate}$ $D_{98,95}$)	FM (+6.5% P+)
2*†‡	CP_{OM}	CP_{COP} (+4.0% $CTV_{prostate}$ $D_{98,95}$)	FM (+1.3% $CTV_{prostate}$ $D_{98,95}$)
3*	CP_{OM}	CP_{COP} (+3.4% $CTV_{prostate}$ $D_{98,95}$)	FM (+2.8% P+)
4*‡	CP_{OM}	CP_{COP} (+7.3% CTV_{SV} $D_{98,95}$)	FM (+1.0% $CTV_{prostate}$ $D_{98,95}$)
5*	CP_{OM}	CP_{COP} (+7.2% CTV_{SV} $D_{98,95}$)	FM (+11.9% P+)
6*	CP_{OM}	CP_{COP} (+1.0% $CTV_{prostate}$ $D_{98,95}$)	FM (+21.5% P+)
7	CP_{COP}	CP_{OM} (−3.2% Rectum, $D_{2,5}$)	FM (+4.2% P+)
8*	CP_{OM}	CP_{COP} (+9.8% CTV_{SV} $D_{98,95}$)	FM (+0.9% P+)
9*†‡	CP_{OM}	CP_{COP} (+7.3% CTV_{SV} $D_{98,95}$)	FM (+5.0% CTV_{SV} $D_{98,95}$)
10*†‡	CP_{COP}	CP_{OM} (+1.2% CTV_{SV} $D_{98,95}$)	FM (+5.5% CTV_{SV} $D_{98,95}$)
11‡	CP_{COP}	CP_{OM} (+5.9% P+)	FM (+1.1% $CTV_{prostate}$ $D_{98,95}$)
12†‡	CP_{COP}	CP_{OM} (+0.8% $CTV_{prostate}$ $D_{98,95}$)	FM (+2.4% $CTV_{prostate}$ $D_{98,95}$)
13	CP_{OM}	CP_{COP} (+2% P+)	FM (+3.1% P+)
14	CP_{OM}	CP_{COP} (−3.1% Rectum, $D_{2,5}$)	FM (+3.3% P+)
15*	CP_{OM}	CP_{COP} (+8.8% $D_{98,95}$)	FM (+22.8% P+)
16‡	CP_{COP}	CP_{OM} (+1.7% P+)	FM (+1.0% $CTV_{prostate}$ $D_{98,95}$)
17*	CP_{OM}	CP_{COP} (+3.9% CTV_{SV} $D_{98,95}$)	FM (+9.5% P+)
18*†‡	CP_{COP}	CP_{OM} (+0.6% $CTV_{prostate}$ $D_{98,95}$)	FM (+0.8% $CTV_{prostate}$ $D_{98,95}$)
19	CP_{COP}	CP_{OM} (−0.6% Rectum $D_{30,5}$)	FM (+6.4% P+)

Two quantities were computed for all zero-PTV plans. One was the percentage dose degradation $\%\Delta D_{98,95}$

$$\%\Delta D_{98,95} = \begin{cases} \dfrac{D_{98,95,Rx} - D_{98,95}}{D_{98,95,Rx}} \cdot 100\% & (D_{98,95} < D_{98,95,Rx}) \\ 0 & (\text{Else}) \end{cases}. \quad (4)$$

The other was the percentage DVH spread $\%\Delta DVH_{98,5\text{-}95}$

$$\%\Delta DVH_{98,5\text{-}95} = \frac{D_{98,5} - D_{98,95}}{(D_{98,5} + D_{98,95})/2} \cdot 100\%. \quad (5)$$

$\%\Delta DVH_{98,5\text{-}95}$ showed how the possible DVHs in different virtual treatment courses scatter within the 90% confidence interval around mean DVH.

2.D.2. *FM vs* CP_{OM} *vs* CP_{COP}

When replanning was required, FM, CP_{OM}, and CP_{COP} were performed and the three plans were compared to determine which planning technique is preferred. The preference criteria were primarily target coverage probabilities corresponding to the optimization objectives. Additionally, the P+ (probability of complication free control) value was examined for a secondary comparison.

$$P+ = E[TCP_{prostate}] \cdot (1 - E[NTCP_{rectum}]) \cdot (1 - E[NTCP_{bladder}]), \quad (6)$$

where the formulas and parameters of TCP and NTCP are listed in Table II. In our probabilistic framework, TCP and NTCP were independently evaluated on the base-CTV structures for each simulated treatment course. From the 1000 treatment course simulations, distributions of TCP and NTCP were evaluated. We believe that using the expectation values of TCP and NTCP had significant advantages with respect to TCP/NTCP evaluations on static geometries since our evaluation was for the actual tissue of interest, e.g., CTV instead of PTV, and it incorporated the effects of organ deformation and other uncertainties when modeled.

3. RESULTS

3.A. Dosimetric effect evaluation on zero-PTV-margin plans

Even with $CTV_{prostate}$ centroid aligned, none of the patients is immune to the degradation effect of target coverage due to deformable organ motions (Table III): 0/19 patients satisfy the $D_{98,95,Rx}$ objective for both $CTV_{prostate}$ and CTV_{SV}, as one or the other $\%\Delta D_{98,95} > 0\%$. The range of $\%\Delta D_{98,95}$ is 0.7%–10.5% for $CTV_{prostate}$ and 0.0%–28.3% for CTV_{SV}, and the range of $\%\Delta DVH_{98,5\text{-}95}$ is 0.2%–2.3% for $CTV_{prostate}$ and 1.4%–16.3% for CTV_{SV}. Though the dosimetric consequence of deformable motions differs from patient to patient, all 19 patients need PTV margins or CP_{COP} to further improve the target dose coverage.

3.B. FM vs CP_{OM} vs CP_{COP}

Among the CP_{COP}, CP_{OM}, FM plans generated for each patient, either (12/19) CP_{OM} plans or (7/19) CP_{COP} plans were preferred (Table IV). The relative advantages between the three plans were patient-specific. The patient-specific clinical benefit of CP plans was significant for some patients. Relative to FM plans, 5/7 CP_{COP} plans and 3/12 CP_{OM} plans

improved target $D_{98,95}$ value up to 5% of the prescribed dose, and 2/7 CP_{COP} and 9/12 CP_{OM} plans achieved better OAR sparing with P+ gain from 0.9%–22.8%. When CP_{COP} and CP_{OM} competed with each other, the advantage of the most preferred plan was either better target coverage or lower OAR dose. 3/7 CP_{COP} plans versus 10/12 CP_{OM} plans improved $D_{98,95}$ values up to 1.2% versus 9.8% of the prescribed dose. 4/7 CP_{COP} plans versus 2/12 CP_{OM} plans resulted in maximum 5.9% versus 2% P+ gain.

When pDVHs and P+ gains were averaged across 19 patients, the advantages of CP_{COP} and CP_{OM} plans relative to FM somewhat canceled out on a population basis because some patients have target coverage improvement or where others have better OAR dose sparing. Still, the average P+ gain of CP_{COP} and CP_{OM} relative to FM was 1.1% and 3.1%, respectively.

TABLE V. The monitor units per fraction for CP_{COP} plans and percentage deviation from CP_{COP} for the CP_{OM} and FM plans.

ID	CP_{COP}	CP_{OM}	FM
1	483	−13	−8
2	448	+29	+20
3	636	−7	−1
4	531	−8	−3
5	489	0	+3
6	401	−6	+4
7	406	−5	+6
8	361	+10	+29
9	440	+70	+8
10	537	+5	−7
11	478	+33	+33
12	565	−5	+2
13	555	−10	+7
14	541	−10	−5
15	434	−8	+11
16	441	−5	+14
17	552	−3	+5
18	476	+6	+23
19	405	+1	+10
Average	483.1	+3	+7

4. DISCUSSION

Coverage probability is an important metric for the evaluation/optimization of plans under the influence of GUs. PTV/PRV margins are the primary method used in current clinics to account for errors and uncertainties in ROIs as these margins are intuitive, simple to implement, and have been extensively studied. For a typical (static) plan, evaluation/optimization is performed on a single image set and coverage is thought of in terms of isodose coverage of a PTV/PRV. Of note, it is ICRU defined treated volume,[12] not PTV/PRV, that dictates coverage. Unlike PTV/PRV margins that may be intended to ensure a prespecified coverage probability,[5] coverage probability provides a probability estimate of achieving isodose coverage. Since computed coverage probabilities often differ considerably from the value implied by margin formulas for PTV-based the static plans,[12,31] coverage probability adds useful information that is missing from current clinical practice.

Acknowledging the challenges presented by daily organ deformations, many research groups have concentrated on developing time-of-treatment adaptive replanning to accommodate errors.[37–41] While adaptive replanning may become the standard, it will only do so if/when is benefits outweigh the drawbacks of the daily reimaging, daily replanning time, and added resources required compared with current practice or other competing methods.

The CP methods described in this paper describe one potential competing method. Like current margin-based approach, it designs treatment beams which can be delivered throughout a radiation therapy course (or subcourse if desired) avoiding the drawbacks of daily replanning. While CP methods may eventually be compared with daily replanning methods to justify replanning dosimetric advantages with respect to CP, the present study justifies CP for deformable organs with respect to the fixed margin approach. In this paper, the CP model is idealized since it presupposes a set of 7–12 patient-specific repeat CT image sets to generate the PCA model. Such number of sets would be unlikely, however, a reduced number of input images might suffice, nonionizing (MR) based image sets, or population based image sets might provide alternatives. Nonetheless, this idealized study is necessary to determine if pursuing these other options is worthwhile. The scope of this work is limited to the interactional deformable motions. Other uncertainties, including setup uncertainties target delineation, are covered in separate studies[13] or future work.

Three planning techniques—CP_{COP}, CP_{OM}, and FM—were used to consider the ROI interfractional deformable motions which naturally occur through the treatment course while achieving the treatment intent. CP_{COP} directly optimizes the dose distribution and yields a dosimetric margin which accommodates modeled geometric uncertainties for CTV and OARs, while both CP_{OM} and FM utilize a surrogate volume PTV and ignores the effect of deformation on OARs during optimization. The PTV size for FM was empirically determined and for CP_{OM} was optimized based on target coverage probability. FM represents the conventional clinical method which is convenient but faces the fundamental problem of how to determine the optimal PTV margins tailored to each patient's characteristics. CP_{OM} represents a simple form of coverage probability-based treatment planning to optimize patient-specific PTV margins. The optimized PTV margins are uniform, without being shaved for OARs.

As expected, when coverage probability is explicitly analyzed during plan optimization (i.e., CP_{COP} and CP_{OM}), the resultant treatment provides better coverage than the FM method. CP techniques show the potential clinical benefit in either target coverage probability or OAR sparing or both (Table IV). On a population based comparison, the advantages of CP techniques relative to FM are not pronounced due to the cancellation of gains in target coverage for some patients and gains in OAR sparing for the others. Overall, the

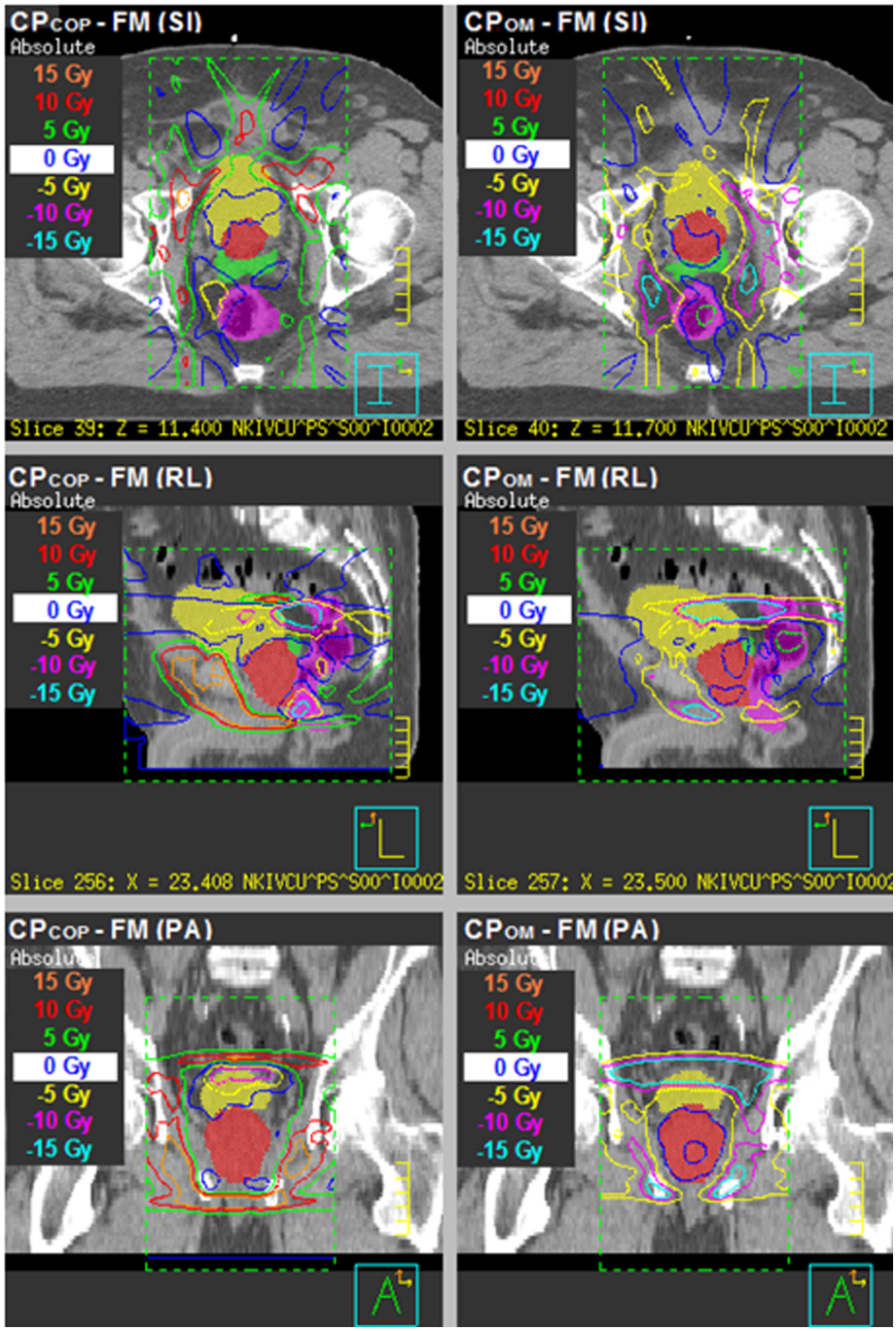

FIG. 3. The simulated dose distribution differences between different plans, CP_{COP} minus FM (left column) and CP_{OM} minus FM (right column), in SI, RL, and PA slices for patient 19 for a single treatment course when deformable organ motion is considered. The ROIs displayed as colorwash are $CTV_{prostate}$ (red), CTV_{SV} (green), bladder (yellow), and rectum (magenta). The dose distribution around $CTV_{prostate}$ in CP_{COP} plan is quite different from that on CP_{OM} and FM plans.

benefit of using CP techniques is patient-specific and can be significant for certain cases.

Another benefit of the CP methods is that plan delivery complexity does not get increased. A simplistic surrogate of treatment plan complexity is the number of monitor units required to achieve the prescription dose.

Table V compares the monitor units per fraction for CP_{COP}, CP_{OM}, and FM techniques. Larger MUs typically indicate an increase in the complexity (number of segments) for the delivery. On average, CP_{COP} requires the fewest MUs, followed by CP_{OM} and FM. If the most deviant CP_{OM} plan (A5) is removed, then CP_{OM} requires on average the same number of MU as CP_{COP}.

When it comes to the relative advantages of CP_{OM} and CP_{COP}, it also shows patient-specific characteristics. As implemented, the CP_{OM} method effectively yields a CTV coverage hard constraint: when the current PTV margins are regarded as too small, they are increased without considering the OAR criteria. In contrast, the flexibility of CP_{COP} yields dose distribution differences with respect to the CP_{OM} and

TABLE VI. Target percentage degraded dose $\%\Delta D_{98,95}$ (%) of CP_{COP}, CP_{OM} or FM plan for patients 1–19 when accommodating deformable motions.

	$\%\Delta D_{98,95}$ of $CTV_{prostate}$			$\%\Delta D_{98,95}$ of CTV_{SV}		
ID	CP_{COP}	CP_{OM}	FM	CP_{COP}	CP_{OM}	FM
1	0.2	0.0	1.4	0.0	0.0	0.0
2	4.1	0.1	1.4	0.0	0.0	0.0
3	2.7	0.0	0.0	0.3	0.0	0.0
4	0.0	0.0	1.0	3.7	0.0	0.0
5	1.0	0.0	0.0	7.2	0.0	0.0
6	0.8	0.0	0.0	0.0	0.0	0.0
7	0.0	0.0	0.0	0.0	0.0	0.0
8	0.0	0.0	0.0	9.3	0.0	0.0
9	3.7	1.1	0.5	7.1	0.0	4.9
10	0.5	1.1	1.2	2.9	4.1	8.4
11	0.0	0.0	0.1	0.0	0.0	0.0
12	0.0	0.6	2.3	0.0	0.0	0.0
13	0.0	0.0	0.0	0.0	0.0	0.0
14	0.0	0.0	0.0	0.0	0.0	0.0
15	1.3	0.0	0.0	7.7	0.0	0.0
16	0.0	0.0	0.2	0.0	0.0	0.0
17	0.9	0.0	0.0	1.5	0.0	0.0
18	0.1	0.0	0.9	0.0	0.4	0.0
19	0.0	0.0	0.0	0.0	0.0	0.0

FM margin-based plans. As Fig. 3 shows, CP_{OM} and FM plans differ little around the $CTV_{prostate}$ volume as indicated by the 0 Gy isodose surface, while this is not the case for the difference between the CP_{COP} and FM plans. In this example, CP_{COP} tends to push dose to the non-OAR region adjacent to the target to ensure target coverage. Since CP_{COP} balances all coverage probabilities for CTVs and OARs that are associated with the optimization criteria, no hard constraint is placed on the CTV coverage. Consequently, CP_{COP} can be compromised to OAR sparing to ensure the composite objective value is minimized. Such compromises eliminated CP_{COP} from contention, when target coverage probability was the primary selection criteria for the preferred plan.

Future implementations to further improve CP technique could consider optimal objective function weights or inclusion of hard constraints. By using the objectives in Table I, Table VI shows that 11/19 CP_{COP} plans and 5/19 CP_{OM} plans (versus 8/19 FM plans) had nonzero $\%\Delta D_{98,95}$ for either $CTV_{prostate}$ or CTV_{SV} and thus failed to meet the optimization criteria of target coverage probability $D_{98,95}$. As discussed, CP_{COP} is most likely to fail the prescribed $D_{98,95}$ mainly because of the selected objective weights of CTVs and OARs. The typical $\%\Delta D_{98,95}$ of a CP_{COP} plan was within 1%, although it could be up to 4.1% for $CTV_{prostate}$ and 9.3% for CTV_{SV}. When the CP_{COP} plan achieved the prescribed $D_{98,95}$, it was most likely to be preferred among the three. As indicated in Fig. 4, preferred objective function weights for CP techniques may be patient and ROI specific. CP_{OM} failed for some patients when PTV margins were expanded to a very large size (Table III), which resulted in overlap volumes between larger PTV, bladder, and rectum.

Figure 5 shows the tendency of the competing target and OAR doses at each prescribed coverage probability using

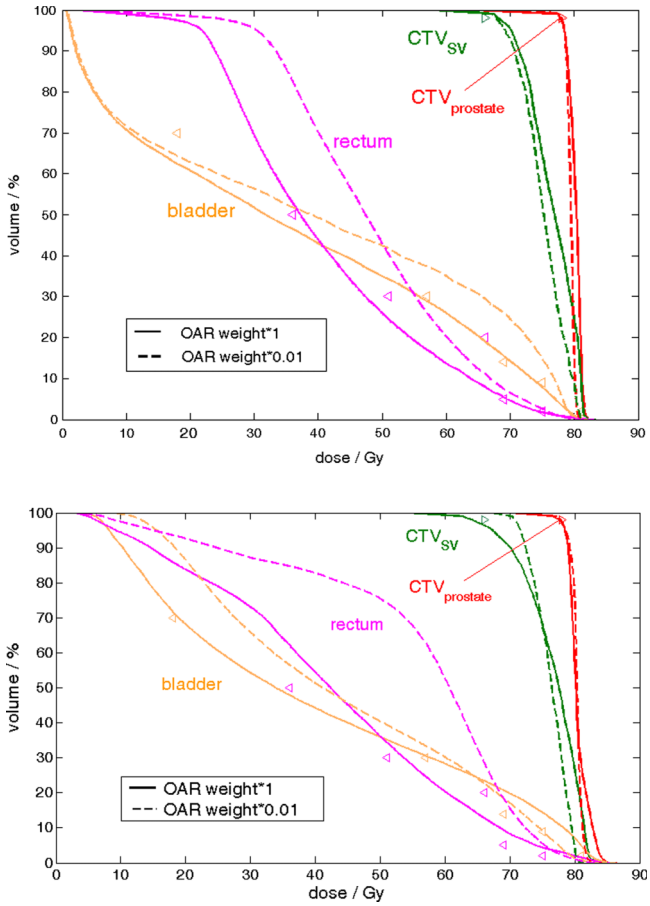

FIG. 4. Examples of the CP_{COP} plans of two patients with ID 1 (upper) and 10 (lower) that use the original OAR objective weights (solid) (listed in Table I) versus reduced OAR objective weights with a factor 0.01 (dashed). The pDVHs are of 95% for $CTV_{prostate}$ (red) and CTV_{SV} (green) and 5% for bladder (orange) and rectum (magenta). Reduced OAR objective weights for these two patient cases result in improved target coverage at the price of OAR doses above the treatment objectives.

different PTV margins. Due to this challenge, increasing uniform PTV margins was not the universal solution to ensure target coverage probability. Still, CP_{OM} reasonably expanded PTVs according to the target coverage probability for most patients and CP_{OM} was much less limited by the selections of objective weights of CTVs and OARs. Nonetheless, CTV coverage would have been achieved if OAR weights were reduced.

To validate that 1000 simulations were sufficient for our coverage calculations, two patients were arbitrarily selected to determine the convergence of $D_{v,q}$ using 10, 100, 200, and 500 virtual treatment courses relative to that using 1000. Denote D_{v,q_Ntx} the estimated $D_{v,q}$ based on N_{tx} virtual treatment courses. For $CTV_{prostate}$ and CTV_{SV}, $D_{98,95\_Ntx}$ relative to $D_{98,95\_1000}$ was $\leq |\pm 0.2|\%$ when N_{tx} is 500. For OARs, the absolute value of the percentage difference remained within 1% (mostly <0.5%) in the high dose region (where v of $D_{v,q}$ was small) and tended to be larger (1%–5%) in the low dose region (where v of $D_{v,q}$ was large). The precision was tested by reproducing each D_{v,q_1000} for 7–10 times. The maximum absolute percentage difference among

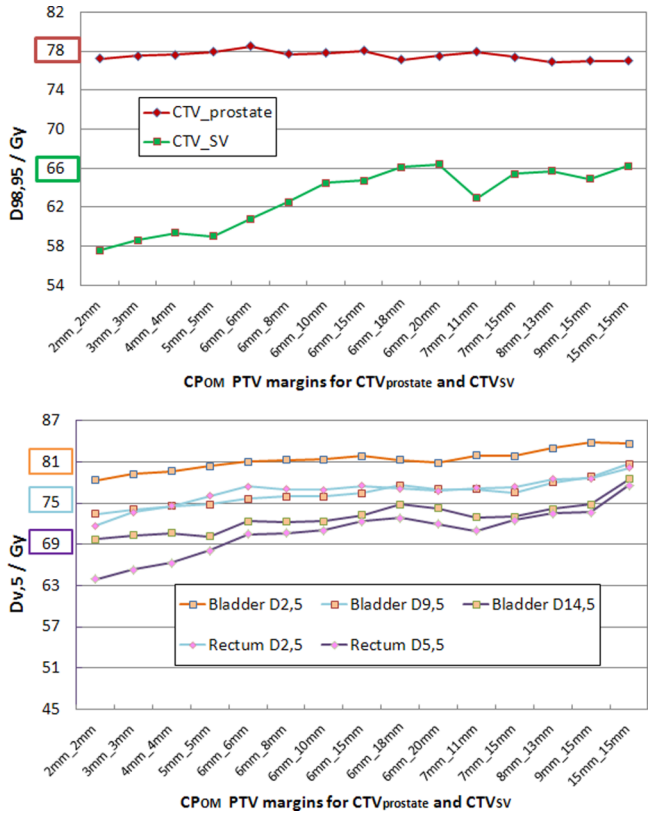

FIG. 5. An example of the increasing competition between target and OAR criteria with increasing PTV margins during CP_{OM} optimization. The target prescribed dose or the OAR tolerance dose is highlighted in the same color as the achieved dose curve for each ROI criterion. On the abscissa, the values are given in the format Xmm_Ymm, where X is the $CTV_{prostate}$ margin and Y is the CTV_{SV} margin.

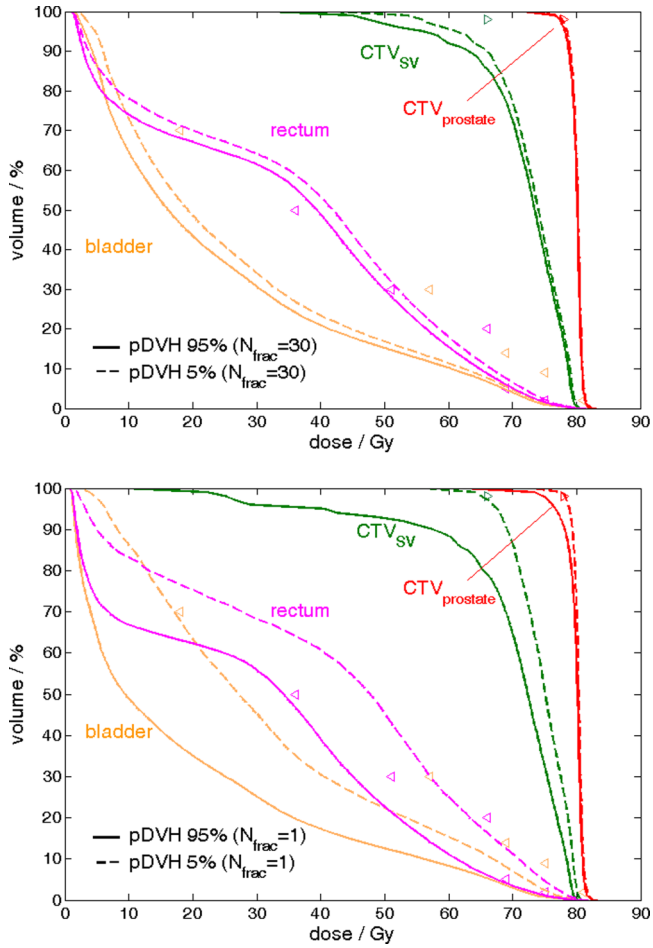

FIG. 6. An example of pDVHs 95% (solid) and pDVHs 5% (dashed) evaluated on a patient treatment case with (upper) 30 fractions (i.e., $N_{frac} = 30$) and (lower) 1 fraction (i.e., $N_{frac} = 1$) for the $CTV_{prostate}$ (red), CTV_{SV} (green), bladder (orange) and rectum (magenta) with optimization objectives (triangle markers). When $N_{frac} \gg 1$, the per voxel dose variability reduces, decreasing the spread in the 95% and 5% pDVHs.

all repeated estimated values was 0.2% for $CTV_{prostate}$, 0.3% for CTV_{SV}, and 3.5% for all OARs. In general, $D_{v,q}$ is more precise in high dose regions. As the low dose region was of less interest in terms of dose sparing and OAR toxicity, these test cases supported that coverage estimation using 1000 virtual treatment courses was adequate. Our finding agreed with study from Söhn *et al.*[21] where 10 000 35-fraction treatment courses were simulated. We both showed that the effects of deformable motions for cumulative plan are smaller than those from a single fraction because hot spot and cold spots in moving voxels cancel out when fraction number is much larger than 1 (Fig. 6).

Although 1000 treatment courses were used for the coverage evaluation, we opted to simulate 100 courses during the optimization to reduce the overall computational burden. While this leads to more optimization iterations due to course-set to course-set statistical variations, trial-and-error testing revealed that 100 in-optimization treatment course simulations were sufficient to ensure convergence and provide a reasonable compromise/reduction in overall computation time, which is approximately proportional to the number of treatment course simulations times the number of optimization iterations. In any event, the final coverage evaluation utilized 1000 virtual treatment courses to iterations to ensure accurate evaluation of the final coverage.

5. CONCLUSION

For the high-risk prostate cancer patients treated with external beam radiation therapy, dosimetric variability caused by interfractional tissue deformation should be considered during treatment planning in order to ensure target coverage and organ sparing. Simulating such deformations via application of PCA model permits evaluation of probability of achieving coverage or avoidance. When these models are utilized within the plan optimization loop, e.g., CP_{COP} and CP_{OM}, improved target dose coverage or lower normal tissue toxicity is achieved compared with fixed PTV margin techniques.

ACKNOWLEDGMENTS

This work was supported in part by NIH Grant No. P01CA116602 and by a research contract with Philips Medical Systems. The authors thank the Netherlands Cancer Institute for providing the image sets, Ford Sleeman and

Dr. Mirek Fatyga for the initial processing of the image sets, Dr. Elizabeth Weiss for contouring the image sets, Dr. Gary Christianson for access and use of the SICLE algorithm, Dr. Jeffrey Williamson and the VCU P01 team for their inputs and stimulating discussion, Dr. Martin J. Murphy for his advice and careful review of the PCA mathematics.

APPENDIX: PRINCIPAL COMPONENT ANALYSIS FOR GENERATION OF 3D DISPLACEMENT VECTOR FIELDS

This section briefly describes the PCA model used to generate the synthetic displacement vector fields (DVFs) utilized to deform the reference planning ROIs to synthetic "per-fraction" ROIs for treatment simulations used to assess the ROI coverage probabilities.

The per-patient PCA model input data consisted of the set of DVFs that relate voxel locations on the reference planning image to point on the repeat FBCT images. The input DVFs were calculated by the deformable registration algorithm called small deformation inverse-consistent linear elastic (SICLE).[42] The registration was based on the grayscale information as well as the contours for prostate, bladder, and rectum. Input DVFs were quality assured via visual inspection of contours plus dice coefficient relative to manual contours.

The PCA model workflow is illustrated in Fig. 1 and is described here for a single patient. Registrations utilizing the N_{rCT} rCTs yielded N_{DVF} DVFs. Prior to PCA input, each DVF was used to form a vector $\mathbf{DVF}_i \in \mathrm{R}^{3N_{vox}\times 1}$ (where $i=\{1,2,\ldots,N_{DVF}\}$) with N_{vox} being the number of DVF voxel elements. $\mathrm{R}^{3N_{vox}\times 1}$ indicates that the size of vector, expressed as a $3N_{vox}$ (rows) by 1 (columns) matrix

$$\mathbf{DVF}_i = (\,x_{1,i}\quad x_{2,i}\quad \cdots\quad x_{N_{vox},i}\quad y_{1,i}\quad y_{2,i}\quad \cdots\quad y_{N_{vox},i}\quad z_{1,i}\quad z_{2,i}\quad \cdots\quad z_{N_{vox},i}\,)^T, \tag{A1}$$

where x,y,z were the displacement vector field components in the x,y,z directions for each DVF voxel and $(\ )^T$ denoted the transpose of the matrix. The systematic component $\mathbf{DVF}_{syst} \in \mathrm{R}^{3N_{vox}\times 1}$ from the $\mathbf{DVF}_i$ set related the patient's average anatomy to the reference image set, and equals the mean of the N_{DVF} DVFs

$$\mathbf{DVF}_{syst} = \frac{1}{N_{DVF}} \sum_{i=1}^{N_{DVF}} \mathbf{DVF}_i. \tag{A2}$$

The residual per-image-set variation from $\mathbf{DVF}_{syst}$ can be cast as "random" components, $\mathbf{DVF}_{rand,i} \in \mathrm{R}^{3N_{vox}\times 1}$, where

$$\mathbf{DVF}_{rand,i} = \mathbf{DVF}_i - \mathbf{DVF}_{syst}. \tag{A3}$$

$\mathbf{DVF}_{rand,i}$ is then composed into $\mathbf{DVF}_{rand} \in \mathrm{R}^{3N_{vox}\times N_{DVF}}$, where each column corresponds with an $\mathbf{DVF}_{rand,i}$.

$$\mathbf{DVF}_{rand} = \left(\mathbf{DVF}_{rand,1}\ \mathbf{DVF}_{rand,2}\ \ldots\ \mathbf{DVF}_{rand,N_{DVF}}\right). \tag{A4}$$

PCA analysis was performed on $\mathbf{DVF}_{rand}$.

For $\mathbf{DVF}_{rand}$, the covariance matrix $\mathbf{C} \in \mathrm{R}^{3N_{vox}\times 3N_{vox}}$ that generalized the notion of variance to dimensions $3N_{vox}\times 3N_{vox}$ (Refs. 43 and 44) is

$$\mathbf{C} = \frac{1}{N_{DVF}} \mathbf{DVF}_{rand} \mathbf{DVF}_{rand}{}^T, \tag{A5}$$

where $(\ )\cdot(\ )^T$ represented the outer product of the two matrices. The diagonalization of $\mathbf{C}$ yields a set of eigenvectors, $\mathbf{V}(l) \in \mathrm{R}^{3N_{vox}\times 1}$, and their associated eigenvalues, $\lambda_l \in \mathrm{R}^{1\times 1}$. These eigenvectors and eigenvalues satisfy the following relation, $\boldsymbol{CV} = \lambda \mathbf{V}$. In practice, the $3N_{vox}\times 3N_{vox}$ covariance matrix is intractable. To reduce the computational burden, $\mathbf{V}$ and λ are calculated using an alternative method useful when $N_{DVF} \ll 3N_{vox}$.[45] First, Eq. (A5) is substituted into the eigenvector equation

$$\frac{1}{N_{DVF}} \mathbf{DVF}_{rand} \mathbf{DVF}_{rand}{}^T \mathbf{V} = \lambda \mathbf{V}. \tag{A6}$$

Multiplying by $\mathbf{DVF}_{rand}{}^T$ and defining $\mathbf{U} = \mathbf{DVF}_{rand}{}^T \mathbf{V}$ gives

$$\frac{1}{N_{DVF}} \mathbf{DVF}_{rand}{}^T \mathbf{DVF}_{rand} \mathbf{U} = \lambda \mathbf{U}. \tag{A7}$$

This permits $\mathbf{U}$ to be calculated as the eigenvectors of the smaller $N_{DVF}\times N_{DVF}$ matrix, $\mathbf{DVF}_{rand}{}^T \mathbf{DVF}_{rand}$. Multiplying both sides of the above equation by $\mathbf{DVF}_{rand}$ gives

$$\frac{1}{N_{DVF}} \mathbf{DVF}_{rand} \mathbf{DVF}_{rand}{}^T (\mathbf{DVF}_{rand}\mathbf{U}) = \lambda (\mathbf{DVF}_{rand}\mathbf{U}). \tag{A8}$$

Thus, the eigenvectors for the full covariance matrix are determined by the relation

$$\mathbf{V}_i = \frac{1}{\sqrt{N_{DVF}\lambda_i}} \mathbf{DVF}_{rand}\mathbf{U}_i, \tag{A9}$$

where $1/\sqrt{N_{DVF}\lambda_i}$ is a factor used to renormalize the computed eigenvectors. These eigenvectors, also called eigenmodes, represent pseudo-DVFs of correlated displacements of N_{vox} voxels. The eigenvectors were mutually independent vector fields and the maximum number of eigenmodes that existed was $N_{DVF}-1$. Therefore, the whole eigenvector matrix was $\mathbf{V} \in \mathrm{R}^{3N_{vox}\times(N_{DVF}-1)}$. To measure the fraction of overall random tissue motion variability represented by an eigenmode with index l, the relative eigenvalue $\bar{\lambda}_l$ was calculated as

$$\bar{\lambda}_l = 100\% \cdot \frac{\lambda_l}{\sum_{i=1,2,\ldots,N_{DVF}} \lambda_i}. \tag{A10}$$

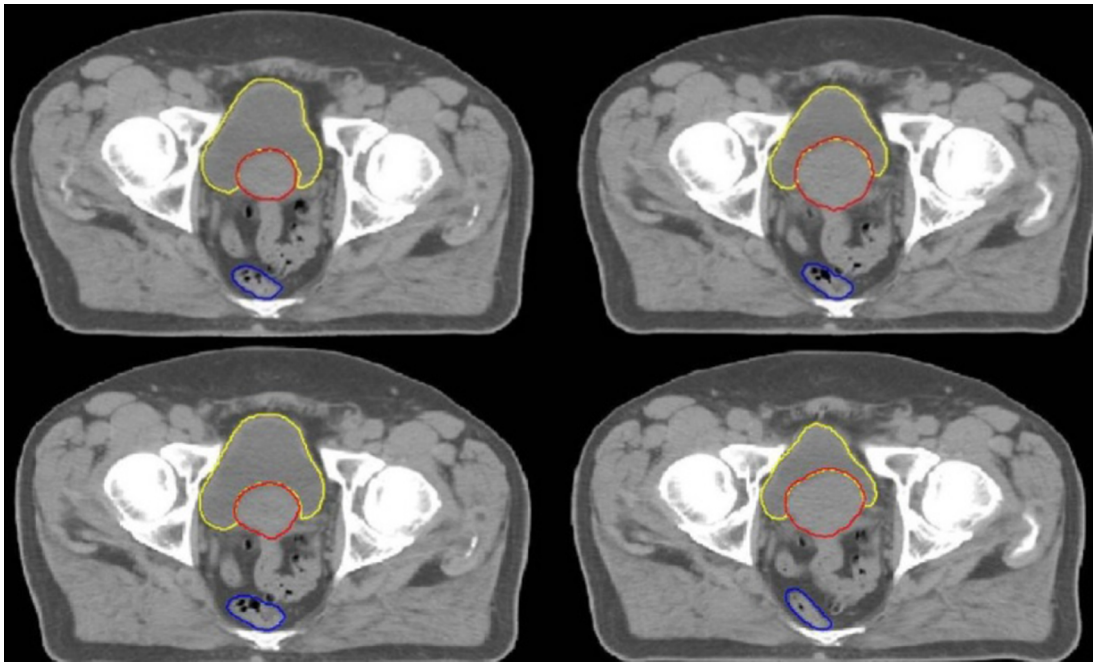

FIG. 7. Four synthetically created PCA geometries for a single patient. Each image shows the same slice of a given patient at four synthetically sampled time points over the patient's treatment course. For illustration purposes, the deformed contours are showed overlaid on the deformed CT images. In this work, only the deformed contours are incorporated into the methodology.

The larger the eigenvalue, the more dominating the eigenmode was due to capturing a larger percentage of the geometric variability in $\mathbf{DVF}_{\text{mat}}$. The total percentage of geometric variability $\bar{\lambda}$ accounted for by the L most "principal" eigenmodes was

$$\bar{\lambda} = \sum_{i=1,2,\ldots,L} \bar{\lambda}_i. \tag{A11}$$

To ensure that the set of synthetic DVFs represented at least 90% of the overall geometric variability, L was determined by $\bar{\lambda} \geq 90\%$ and consequently ranged from 4 to 7 for the 19 patients.

For each eigenvector, coefficients were found in a matrix $\mathbf{Coeff} \in \mathrm{R}^{N_{\text{DVF}} \times (N_{\text{DVF}}-1)}$, which was the product of $\mathbf{DVF}_{\text{rand}}{}^{T}$ and eigenvector matrix $\mathbf{V}$

$$\mathbf{Coeff} = (\mathbf{DVF}_{\text{rand}})^{T}\mathbf{V} = \begin{pmatrix} c_{1,1} & \cdots & c_{l,1} & \cdots & c_{N_{\text{DVF}-1},1} \\ \vdots & \ddots & \cdots & \iddots & \vdots \\ c_{1,i} & \cdots & c_{l,i} & \cdots & c_{N_{\text{DVF}-1},i} \\ \vdots & \iddots & \cdots & \ddots & \vdots \\ c_{1,N_{\text{DVF}}} & \cdots & c_{l,N_{\text{DVF}}} & \cdots & c_{N_{\text{DVF}-1},N_{\text{DVF}}} \end{pmatrix}, \tag{A12}$$

where i and l were the row and the column indexes of **Coeff** corresponding to $\mathbf{DVF}_{\text{rand}}(i)$ and $\mathbf{V}(l)$. Based on this finite data sample of eigenvector coefficients **Coeff**, a probability density function (PDF) for the lth eigenvector could be estimated by kernel density estimation (KDE).[46–49] For the lth eigenvector, the PDF P_l of random variable t was represented using a Gaussian kernel

$$P_l[a \leq t \leq b] = \frac{1}{N_{\text{DVF}} \cdot \sigma_l \cdot \sqrt{2\pi}} \sum_{i=1}^{N_{\text{DVF}}} e^{-(t-c_{i,l})^2/2\sigma_l^2}, \tag{A13}$$

where $c_{i,l}$ was the matrix **Coeff** element in the ith row and the lth column in Eq. (A12). For sampling purposes, the PDF is calculated over the symmetric range a to b, where these cutoff parameters were chosen to ensure that $P_l[a]$ and $P_l[b] < 0.0001 \max[P_l]$. The Gaussian SD σ_l was determined using the rule of thumb equation.[50]

$$\sigma_l = \frac{1.06}{N_{\text{DVF}}{}^{0.2}} \sqrt{\frac{\sum_i^{N_{\text{DVF}}} (c_{i,l} - \frac{1}{N_{\text{DVF}}} \sum_i^{N_{\text{DVF}}} c_{i,l})^2}{N_{\text{DVF}} - 1}}. \tag{A14}$$

The eigenvectors create a new orthogonal basis for the input DVFs. Thus, without loss of generality, any $\mathbf{DVF}_{\mathrm{rand},i}$ can be represented as a linear combination of scalar expansion coefficients, $c_{l,i}$, and their associated eigenvectors, $\mathbf{V}(l)$. As the eigenvectors are uncorrelated, synthetic DVFs, $\mathbf{DVF}_{\mathrm{syn}} \in \mathrm{R}^{3N_{\mathrm{vox}}\times 1}$, can be created by sampling a set of expansion coefficients, α, from the PDFs calculated in Eq. (A13). The synthetic DVFs can then be calculated as

$$\mathbf{DVF}_{\mathrm{syn}} = \mathbf{DVF}_{\mathrm{syst}} + \sum_{l=1}^{L} \alpha_l \cdot \mathbf{V}(l). \tag{A15}$$

In this work, rejection sampling was used to select α_l. This method of making samples of synthetic DVFs from PCA eigenvectors and statistical distributions of expansion coefficients was adapted from Murphy *et al.*[49]

As current clinical practice uses soft tissue target alignment for treatments, the bony-anatomy aligned $\mathbf{DVF}_{\mathrm{syn}}$ generated by the afore developed PCA model were translated to $\mathrm{CTV}_{\mathrm{prostate}}$ centroid aligned DVF. Let the vector element of $\mathbf{DVF}_{\mathrm{syn}}$ be represented by $(x_{\mathrm{syn},i}, y_{\mathrm{syn},i}, z_{\mathrm{syn},i})$, where $i = 1,2,\ldots,N_{\mathrm{vox}}$ and denote synthetic $x_{\mathrm{syn},P}, y_{\mathrm{syn},P}, z_{\mathrm{syn},P}$ as displacement vector of $\mathrm{CTV}_{\mathrm{prostate}}$ centroid. The synthetic DVF for $\mathrm{CTV}_{\mathrm{prostate}}$ centroid-aligned anatomies $\mathbf{DVF}_{\mathrm{syn\_Paligned}} \in \mathrm{R}^{3N_{\mathrm{vox}}\times 1}$ was

$$\mathbf{DVF}_{\mathrm{syn\_Paligned}} = \begin{pmatrix} x_{\mathrm{syn},1} - x_{\mathrm{syn},P} \\ x_{\mathrm{syn},2} - x_{\mathrm{syn},P} \\ \cdots \\ x_{\mathrm{syn},N_{\mathrm{vox}}} - x_{\mathrm{syn},P} \\ y_{\mathrm{syn},1} - y_{\mathrm{syn},P} \\ y_{\mathrm{syn},2} - y_{\mathrm{syn},P} \\ \cdots \\ y_{\mathrm{syn},N_{\mathrm{vox}}} - y_{\mathrm{syn},P} \\ z_{\mathrm{syn},1} - z_{\mathrm{syn},P} \\ z_{\mathrm{syn},2} - z_{\mathrm{syn},P} \\ \cdots \\ z_{\mathrm{syn},N_{\mathrm{vox}}} - z_{\mathrm{syn},P} \end{pmatrix}. \tag{A16}$$

The PCA model generated sets of $\mathbf{DVF}_{\mathrm{syn\_Paligned}}$ for use in the postplanning evaluation to judge/compare treatment plans and in the $\mathrm{CP}_{\mathrm{OM}}/\mathrm{CP}_{\mathrm{COP}}$ optimization processes.

The PCA generated synthetic DVFs for this study were validated using several methods. Initially, statistical characteristics of several synthetic DVFs were compared with those of the input data sets. For large-scale validation, 1000 synthetic ROI sets were generated to permit comparison of distributions of synthetic ROI characteristics (centroid location, volume) with respect to those from the input image sets. For example, the distributions of synthetically derived and the manually derived ROI centroid locations were compared for any significant deviations ($p < 0.05$) using a two sample t-test, the Mann–Whitney **U** test, and the Kolmogorov–Smirnov test. No significant deviations were found between the two distributions in any direction. Additionally, visual inspection of several synthetic prostate, bladder, and rectum regions of interest (ROIs) to ensure they appeared realistic and similar to the ROIs contoured on the input images (Fig. 7).

In terms of the number of PCA input image sets required, others have addressed the minimum number of input geometries to adequately model patient-individual dosimetric variability using PCA. Söhn *et al.*[21] stated that 2–6 dominating eigenmodes[51] are sufficient for modeling and mathematically 3–7 input geometries are required to obtain a proper estimation for these eigenmodes. A head and neck cancer study which used PCA modeling showed that dose estimation accuracy after first three weeks of treatment of cancer was within 1% for most of organs and that the geometric variations can be represented by 3–4 dominating eigenmodes.[25] Therefore, CP application with a limited set (e.g., 4–7 eigenmodes for ≥90% of variability in this work) is plausible.

[a]Author to whom correspondence should be addressed. Electronic mail: hjxu111@gmail.com; Telephone: 410-328-3472; Fax: 410-328-2618.

[1]C. Peng, E. Ahunbay, G. Chen, S. Anderson, C. Lawton, and X. A. Li, "Characterizing interfraction variations and their dosimetric effects in prostate cancer radiotherapy," Int. J. Radiat. Oncol., Biol., Phys. **79**(3), 909–914 (2010).
[2]T. E. Byrne, "A review of prostate motion with considerations for the treatment of prostate cancer," Med. Dosim. **30**(3), 155–161 (2005).
[3]A. M. Nichol *et al.*, "A magnetic resonance imaging study of prostate deformation relative to implanted gold fiducial markers," Int. J. Radiat. Oncol., Biol., Phys. **67**(1), 48–56 (2007).
[4]E. M. Kerkhof, R. W. van der Put, B. W. Raaymakers, U. A. van der Heide, M. van Vulpen, and J. J. W. Lagendijk, "Variation in target and rectum dose due to prostate deformation: An assessment by repeated MR imaging and treatment planning," Phys. Med. Biol. **53**(20), 5623–5634 (2008).
[5]M. van Herk, "Errors and margins in radiotherapy," Semin. Radiat. Oncol. **14**(1), 52–64 (2004).
[6]ICRU Report 50, Prescribing, Recording and Reporting Photon Beam Therapy (ICRU Publications, Bethesda, MD, 1994).
[7]ICRU Report 62, Prescribing, Recording and Reporting Photon Beam Therapy (Supplement to ICRU Report 50) (ICRU Publications, Bethesda, MD, 2000).
[8]J. C. Stroom *et al.*, "Internal organ motion in prostate cancer patients treated in prone and supine treatment position," Radiother. Oncol. **51**(3), 237–248 (1999).
[9]M. van Herk, P. Remeijer, C. Rasch, and J. V. Lebesque, "The probability of correct target dosage: Dose-population histograms for deriving treatment margins in radiotherapy," Int. J. Radiat. Oncol., Biol., Phys. **47**(4), 1121–1135 (2000).
[10]G. J. Meijer *et al.*, "What CTV-to-PTV margins should be applied for prostate irradiation? Four-dimensional quantitative assessment using model-based deformable image registration techniques," Int. J. Radiat. Oncol., Biol., Phys. **72**(5), 1416–1425 (2008).
[11]T. F. Mutanga, H. C. J. de Boer, G. J. van der Wielen, M. S. Hoogeman, L. Incrocci, and B. J. M. Heijmen, "Margin evaluation in the presence of deformation, rotation, and translation in prostate and entire seminal vesicle irradiation with daily marker-based setup corrections," Int. J. Radiat. Oncol., Biol., Phys. **81**(4), 1160–1167 (2011).
[12]J. J. Gordon and J. V. Siebers, "Evaluation of dosimetric margins in prostate IMRT treatment plans," Med. Phys. **35**(2), 569–575 (2008).
[13]J. J. Gordon and J. V. Siebers, "Coverage-based treatment planning: Optimizing the IMRT PTV to meet a CTV coverage criterion," Med. Phys. **36**(3), 961–973 (2009).
[14]J. J. Gordon, N. Sayah, E. Weiss, and J. V. Siebers, "Coverage optimized planning: Probabilistic treatment planning based on dose coverage histogram criteria," Med. Phys. **37**(2), 550–563 (2010).
[15]G. S. Mageras *et al.*, "A method of incorporating organ motion uncertainties into three-dimensional conformal treatment plans," Int. J. Radiat. Oncol., Biol., Phys. **35**(2), 333–342 (1996).
[16]D. Yan, D. A. Jaffray, and J. W. Wong, "A model to accumulate fractionated dose in a deforming organ," Int. J. Radiat. Oncol., Biol., Phys. **44**(3), 665–675 (1999).

[17]E. Fontenla, C. A. Pelizzari, J. C. Roeske, and G. T. Chen, "Using serial imaging data to model variabilities in organ position and shape during radiotherapy," Phys. Med. Biol. **46**(9), 2317–2336 (2001).
[18]M. S. Hoogeman, M. van Herk, D. Yan, L. J. Boersma, P. C. M. Koper, and J. V. Lebesque, "A model to simulate day-to-day variations in rectum shape," Int. J. Radiat. Oncol., Biol., Phys. **54**(2), 615–625 (2002).
[19]M. Söhn, M. Birkner, D. Yan, and M. Alber, "Modelling individual geometric variation based on dominant eigenmodes of organ deformation: Implementation and evaluation," Phys. Med. Biol. **50**(24), 5893–5908 (2005).
[20]E. Budiarto *et al.*, "A population-based model to describe geometrical uncertainties in radiotherapy: Applied to prostate cases," Phys. Med. Biol. **56**(4), 1045–1061 (2011).
[21]M. Söhn, B. Sobotta, and M. Alber, "Dosimetric treatment course simulation based on a statistical model of deformable organ motion," Phys. Med. Biol. **57**(12), 3693–3709 (2012).
[22]G. J. Price and C. J. Moore, "A method to calculate coverage probability from uncertainties in radiotherapy via a statistical shape model," Phys. Med. Biol. **52**(7), 1947–1965 (2007).
[23]K. E. I. Deurloo *et al.*, "Quantification of shape variation of prostate and seminal vesicles during external beam radiotherapy," Int. J. Radiat. Oncol., Biol., Phys. **61**(1), 228–238 (2005).
[24]M. Sharma, E. Weiss, and J. V. Siebers, "Dose deformation-invariance in adaptive prostate radiation therapy: Implication for treatment simulations," Radiother. Oncol. **105**(2), 207–213 (2012).
[25]X. Nie, J. Liang, and D. Yan, "Organ sample generator for expected treatment dose construction and adaptive inverse planning optimization," Med. Phys. **39**(12), 7329–7337 (2012).
[26]Q. Wu and R. Mohan, "Algorithms and functionality of an intensity modulated radiotherapy optimization system," Med. Phys. **27**(4), 701–711 (2000).
[27]A. E. Nahum and D. Tait, "Maximising local control by customised dose prescription for pelvic tumours," in *Advanced Radiation Therapy Tumour Response Monitoring and Treatment Planning* (Springer-Verlag, Heidelberg, 1992), pp. 425–431.
[28]A. Niemierko and M. Goitein, "Implementation of a model for estimating tumor control probability for an inhomogeneously irradiated tumor," Radiother. Oncol. **29**(2), 140–147 (1993).
[29]S. Webb and A. E. Nahum, "A model for calculating tumour control probability in radiotherapy including the effects of inhomogeneous distributions of dose and clonogenic cell density," Phys. Med. Biol. **38**(6), 653–666 (1993).
[30]B. Sanchez-Nieto and A. E. Nahum, "The delta-TCP concept: A clinically useful measure of tumor control probability," Int. J. Radiat. Oncol., Biol., Phys. **44**(2), 369–380 (1999).
[31]R. Cheung *et al.*, "Dose-response characteristics of low- and intermediate-risk prostate cancer treated with external beam radiotherapy," Int. J. Radiat. Oncol., Biol., Phys. **61**(4), 993–1002 (2005).
[32]J. T. Lyman, "Complication probability as assessed from dose-volume histograms," Radiat. Res. Suppl. **8**, S13–S19 (1985).
[33]R. de Crevoisier *et al.*, "Increased risk of biochemical and local failure in patients with distended rectum on the planning CT for prostate cancer radiotherapy," Int. J. Radiat. Oncol., Biol., Phys. **62**(4), 965–973 (2005).
[34]C. Burman, G. J. Kutcher, B. Emami, and M. Goitein, "Fitting of normal tissue tolerance data to an analytic function," Int. J. Radiat. Oncol., Biol., Phys. **21**(1), 123–135 (1991).
[35]G. Luxton, S. L. Hancock, and A. L. Boyer, "Dosimetry and radiobiologic model comparison of IMRT and 3D conformal radiotherapy in treatment of carcinoma of the prostate," Int. J. Radiat. Oncol., Biol., Phys. **59**(1), 267–284 (2004).
[36]H. Xu, J. J. Gordon, and J. V. Siebers, "Sensitivity of post-planning target and OAR coverage estimates to dosimetric margin distribution sampling parameters," Med. Phys. **38**(2), 1018–1027 (2011).
[37]S. S. Park *et al.*, "Adaptive image-guided radiotherapy (IGRT) eliminates the risk of biochemical failure caused by the bias of rectal distension in prostate cancer treatment planning: Clinical evidence," Int. J. Radiat. Oncol., Biol., Phys. **83**(3), 947–952 (2012).
[38]M. Ghilezan, D. Yan, and A. Martinez, "Adaptive radiation therapy for prostate cancer," Semin. Radiat. Oncol. **20**(2), 130–137 (2010).
[39]M. Ghilezan, D. Yan, J. Liang, D. Jaffray, J. Wong, and A. Martinez, "Online image-guided intensity-modulated radiotherapy for prostate cancer: How much improvement can we expect? A theoretical assessment of clinical benefits and potential dose escalation by improving precision and accuracy of radiation delivery," Int. J. Radiat. Oncol., Biol., Phys. **60**(5), 1602–1610 (2004).
[40]T. Li *et al.*, "Adaptive prostate IGRT combining online re-optimization and re-positioning: A feasibility study," Phys. Med. Biol. **56**(5), 1243–1258 (2011).
[41]R. Varadhan, S. K. Hui, S. Way, and K. Nisi, "Assessing prostate, bladder and rectal doses during image guided radiation therapy–need for plan adaptation?" J. Appl. Clin. Med. Phys. **10**(3), 56–74 (2009).
[42]G. E. Christensen and H. J. Johnson, "Consistent image registration," IEEE Trans. Med. Imaging **20**(7), 568–582 (2001).
[43]H. Murakami and B. V. K. V. Kumar, "Efficient calculation of primary images from a set of images," IEEE Trans. Pattern Anal. Mach. Intell. **4**(5), 511–515 (1982).
[44]C. Lorenz and N. Krahnstöver, "Generation of point-based 3D statistical shape models for anatomical objects," Comput. Vis. Image Underst. **77**(2), 175–191 (2000).
[45]C. Bishop, *Pattern Recognition and Machine Learning* (Springer, New York, NY, 2007).
[46]M. Rosenblatt, "Remarks on some nonparametric estimates of a density function," Ann. Math. Statist. **27**(3), 832–837 (1956).
[47]E. Parzen, "On estimation of a probability density function and mode," Ann. Math. Statist. **33**(3), 1065–1076 (1962).
[48]Q. Chen, R. J. Wynne, P. Goulding, and D. Sandoz, "The application of principal component analysis and kernel density estimation to enhance process monitoring," Control Eng. Pract. **8**(5), 531–543 (2000).
[49]M. J. Murphy, F. J. Salguero, J. V. Siebers, D. Staub, and C. Vaman, "A method to estimate the effect of deformable image registration uncertainties on daily dose mapping," Med. Phys. **39**(2), 573–580 (2012).
[50]B. W. Silverman, *Density Estimation for Statistics and Data Analysis* (CRC Press, New York, 1986).
[51]Supported by http://iopscience.iop.org/0031-9155/57/12/3693/media.